Engineering Structures 197 (2019) 109443

Contents lists available at ScienceDirect

Engineering Structures

journal homepage: www.elsevier.com/locate/engstruct

Experimental study on the flexural behavior of concrete beams reinforced with bundled hybrid steel/FRP bars

Zeyang Sun[a], Linchen Fu[a], De-Cheng Feng[a], Apete R. Vatuloka[a], Yang Wei[b], Gang Wu[a,c,*]

[a] Southeast University, Key Laboratory of Concrete and Prestressed Concrete Structures of the Ministry of Education, Nanjing 210096, China
[b] School of Civil Engineering, Nanjing Forestry University, Nanjing 210037, China
[c] National-Local Joint Engineering Research Center for Basalt Fiber Manufacturing and Its Applied Technology, Southeast University, Nanjing 210019, China

ARTICLE INFO

Keywords:
Hybrid steel/FRP bar
Concrete beam
Bundled reinforcement
Strain distribution
Ductility

ABSTRACT

Fiber-reinforced polymers (FRPs) are widely used in the strengthening of concrete structures due to their light weight, high strength, and good durability. For precast concrete structures, bundled FRP/steel bars can substantially ease the construction process. In this paper, experimental studies were conducted on five concrete beams with different types of bundled reinforcements. The test results showed that all the beams exhibited concrete crushing failure modes after the steel bar yielded, and the plastic development of the steel bar was restrained by the elastic FRP bar. As the reinforcement concentration increased, the bond behavior between the longitudinal reinforcement and the surrounding concrete decreased; the postcracking stiffness and crack quantity of the corresponding concrete beam decreased, whereas the crack width increased. Both the initial stiffness and postyield stiffness of the concrete beam with 3-bar bundles were approximately 50% of that of the beam with double-bar bundles. The displacement ductilities of all the concrete beams were greater than six. Due to the differences in the bond behavior, the ultimate displacements of the beams with 3-bar bundles and 6-bar bundles were approximately 1.6 and 1.9 times the ultimate displacement of the beam with single-bar reinforcement, respectively.

1. Introduction

A large number of laborers and a large quantity of formwork are needed in the construction of cast-in-place concrete structures, in which the use of tremendous formwork inevitably affects the environment, and the labor cost continually increases with economic development [1]. Prefabrication of components/members in the factory can greatly reduce the on-site labor requirements, and the construction speed and the quality of the structure can be ensured [2,3]. When the conjunction of a precast concrete member is not well treated, steel bar corrosion will develop very fast, and the corresponding structural performance will be degraded [4]. Fiber-reinforced polymer (FRP) is a kind of composite with high strength, low density, and high durability that can be placed near the corner of the concrete cover to delay the deterioration of the structure from corrosion [5].

In terms of hybrid reinforcement, experimental studies on concrete beams reinforced by FRPs and steel bars have been conducted [6,7]. The longitudinal reinforcements were made of steel bars and glass FRP (GFRP) bars, which were arranged in different layers on the concrete beam sections. The results showed that the yielding of the steel bar can ensure ductility, and the high strength of the FRP improves the bearing capacity of the beam. Tests of twenty-four concrete beams reinforced by steel bars, GFRP bars or hybrid steel/GFRP bars (GFRP bars were placed on the outer tension side) have been conducted [8,9]. These studies found that the failure modes of the hybrid reinforced beams were concrete crushing after the steel yielded, the hybrid reinforced beams had better ductility than the beams reinforced by pure FRP bars, and according to ACI 440.1R-06 [10], the minimum reinforcement ratio for an FRP-reinforced beam could be reduced by 25%. Regarding the seismic performance of a concrete structure, due to the elastoplastic characteristics of ordinary steel bars, the deformation of a reinforced concrete (RC) structure after yielding cannot be effectively controlled [11], and the failure probability of the structure will subsequently increase [12]. Under a stable load that is greater than the yield load, the damage in a concrete column is mainly concentrated on the plastic hinge near the column foot, and the residual deformation would be excessively large after an earthquake [13]; thus, the column collapses more easily during the aftershocks [14,15]. The numerical analysis by

* Corresponding author at: Southeast University, Key Laboratory of Concrete and Prestressed Concrete Structures of the Ministry of Education, Nanjing 211189, China.
E-mail address: g.wu@seu.edu.cn (G. Wu).

https://doi.org/10.1016/j.engstruct.2019.109443
Received 14 March 2019; Received in revised form 11 July 2019; Accepted 23 July 2019

Pettinga et al. [16] shows that under the same unloading displacement, the larger the secondary stiffness (postyield stiffness) is, the smaller the residual displacement of the concrete column, and when the secondary stiffness ratio (ratio of the secondary stiffness to the initial stiffness) of the column exceeds 5%, the residual displacement will be significantly reduced. The emergence of various mechanical properties of FRPs has made it possible to develop structures with stable secondary stiffness [17,18], and a new kind of factory produced rebar, which are referred to as steel-FRP composite bars (SFCBs), was designed for concrete structures to achieve high mechanical performance and good durability [19] through the reinforcement of steel bars and FRP bars; due to the high strength of FRP bars, the reserve of the postyield load carrying capacity of a concrete beam can be improved [20]. An experimental study of concrete columns confined by hybrid steel spirals and FRPs showed that a larger ultimate strain of the confining materials can lead to a higher ultimate deformation capacity [21]. Experimental studies on SFCB-reinforced concrete beams were carried out by the author's research group [22], in which the effective secondary stiffness of SFCB-reinforced beams was verified; the ductility of the hybrid reinforced column can be larger than that of an ordinary RC column [23]. The calculation method for the load-displacement relationship of the hybrid reinforced simply supported concrete beam was proposed by Pang et al. [24], and a new ductility coefficient was proposed. Forty-six beams reinforced by hybrid steel-FRP bars and concrete beams strengthened by near-surface mounted FRP bars were analyzed by Kara et al. [25], and they proposed a numerical technique to predict both the pre- and postcracking deflections of concrete beams. As far as multispan hybrid (FRP and steel) reinforced concrete beams is concerned, a numerical procedure for the determination of the deformation was proposed by Dundar et al. [26], in which the effective flexibilities of members in the cracked state can be considered. Experimental studies were conducted on eight two-span continuous concrete beams, and the results showed that the theoretical method can accurately predict the experimental data [27].

For structures with heavy loads or those designed to resist rare earthquakes, the reinforcement ratio would be relatively large, and the assembly of the beam-column joint would be complicated. Therefore, it is necessary to bundle the longitudinal reinforcement to reduce the difficulty of on-site assembly construction [28]. According to the ACI code [29], the number of bundled bars shall be limited to four, and the cutoffs within the bundles need to be staggered. To study the influence of different methods of bundling hybrid longitudinal reinforcement (FRP bar and steel bar) on the behavior of concrete beams, this paper introduces test results of concrete beams with different reinforcement methods. In this study, two single-reinforcement concrete beams (separate reinforcements) and three concrete beams with different bundled reinforcements were investigated. Related research can provide a basis for the design of bearing capacity and deformation capacity of concrete beams reinforced by bundled composite reinforcements.

2. Experimental study

2.1. Specimen design

The test specimens were all designed as simply supported beams with a rectangular cross-section (220 mm × 300 mm). The total length of the beam was 2200 mm (Fig. 1), of which the pure bending length was 600 mm, and the concrete cover was 20 mm. The hanging bars were made of two HRB335 steel bars with a diameter of 10 mm; the stirrups were made of round steel bars with a diameter of 8 mm, which had an 80 mm spacing and a 135° hook.

The average compressive strength of the three concrete cubes (150 mm × 150 mm × 150 mm) [30] was approximately 43 MPa. There are two types of bars used in this test: HRB400 steel bars and basalt FRP (BFRP) bars (Fig. 2). The basic mechanical properties of the reinforcement are shown in Table 1, in which "Φ10" means the

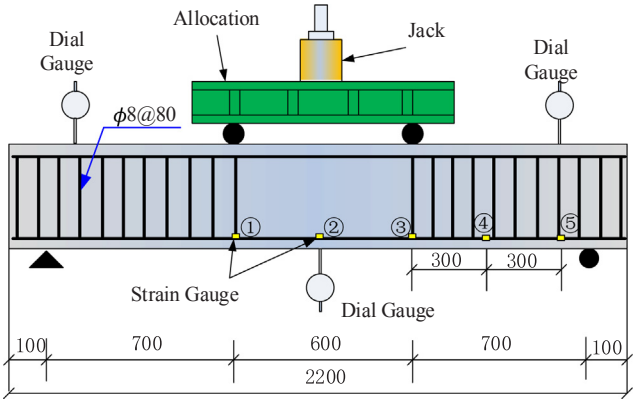

Fig. 1. Design and loading diagram of the test specimen (unit: mm).

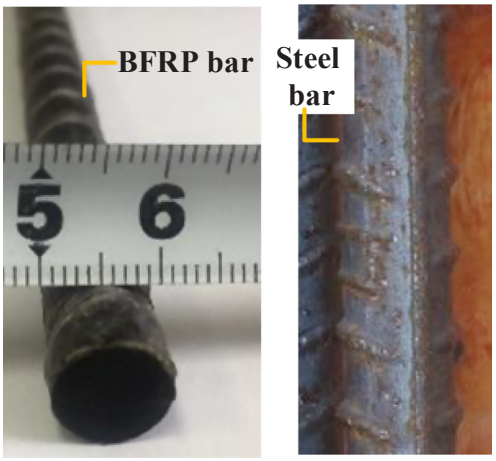

Fig. 2. BFRP bar and steel bar used in the concrete beams.

diameter of the steel bar is 10 mm, "B49" means that the BFRP bar is composed of 49 bundles of 4000 tex basalt fiber, "tex" is the weight of a single bundle fiber per kilometer (g). Note that the width of the surface rib of the BFRP bar is approximately 3.5 mm, and the rib spacing is approximately 12 mm.

The reinforcement ratio of all the beams is the same, and the equivalent reinforcement ratio (ρ_{sf}^{e}) based on the elastic modulus of the steel is 0.56%. Note that ρ_{sf}^{e} is calculated according to Eq. (1).

$$\rho_{sf}^{e} = \frac{{}^{E_f A_f}/_{E_s} + A_s}{A_g} \tag{1}$$

where E_f and A_f are the elastic modulus and cross-sectional area of the FRP bars, respectively; E_s and A_s are the elastic modulus and cross-sectional area of the steel bars, respectively; and A_g is the total cross-sectional area of the concrete beam.

The arrangement of the longitudinal reinforcement in each beam is as follows (Fig. 3). The tensile reinforcement of L-1 is evenly arranged on the same layer, and the spacing is approximately 21 mm. The tensile reinforcement of L-2 is arranged in two layers, wherein the FRP bars (B49) are arranged in the outer layer; the horizontal spacing of the reinforcements in L-2 is approximately 67 mm, and the inner steel bar is approximately 40 mm from the outer FRP bar. The steel bars and FRP bars of L-3 are concentrated into one bundle by thin steel wires, and the distance between the two bundles is approximately 124 mm. The two longitudinal bars (FRP bar and steel bar) of beam L-4 are vertically arranged in a group, and the bar spacing of L-4 is similar to that of L-2. The difference between L-4 and L-2 is that there is no vertical gap between the steel bar and the FRP bar in L-4. The six longitudinal bars of L-5 are concentrated into one bundle, in which the steel bars are

Table 1
Mechanical properties of the steel bars and BFRP bars.

Reinforcement type	Diameter (mm)	Yield strength (MPa)	Elastic modulus (GPa)	Ultimate strength (MPa)	Elongation rate (%)
Steel bar Φ10	10	400	200	585	15
BFRP bar (B49)	10	/	49	1145	2.35

arranged on the inner side, the FRP bars are arranged on the outer side, and the bar edges are approximately 67 mm away from the stirrups on both sides.

2.2. Specimen casting and measurement

Before bundling the main reinforcements, first polish the strain gauge attachment position on the bars. After attaching the strain gauges, the strain gauges are wrapped with resin-impregnated gauze (Fig. 4a); five strain gauges are attached to each longitudinal bar (Fig. 1). A 5 kN preloading step is performed in the test preparation stage to eliminate the error of the actuator displacement at the initial stage of loading. All measurement data are set to the initial state after the test machine load returns to zero.

To clearly obtain the development process of the crack, the test beam was whitened before the test, and then grid lines with a vertical and horizontal spacing of 50 mm were drawn on the side and bottom of the beam. The crack development of the test beam was observed after each stage of loading. Before the beam yielded, to capture the crack point, the loading was applied under force control mode (5 kN /min). After the concrete beam yielded, the number of cracks remained approximately stable, and the load decreased dramatically when the FRP ruptured. As a result, the beam was loaded in displacement control mode (2 mm/min), and three linear variable displacement transformers (LVDTs) were arranged in the two seats and the middle span of the test beam. The location of each LVDT is shown in Fig. 1.

3. Test results

3.1. Test phenomena

The failure modes of the test specimens were concrete crushing in the compression zone after the steel bar yielded without the rupture of the FRP bar. The failure process could be divided into three stages (Fig. 5): a precracking stage (elastic stage), after concrete cracking and before steel bar yielding, and a postyield stage of the steel bar until concrete crushing. In the elastic state before the concrete cracked, the stress of the reinforcement increased linearly with increasing load, and the neutral axis was basically at the middle of the section. After the concrete cracked, as the load increased, the stiffness of the beam decreased and remained stable (approximately linear) until the steel bar yielded, and cracks gradually appeared in the pure bending zone of the concrete beam. When the concrete in the compression zone reached the ultimate compressive strain, the surface of the concrete appeared to peel off and was gradually crushed, and the beam reached the ultimate load.

The damage process of each beam is as follows:

(1) L-1

The damage of beam L-1 is shown in Fig. 6. When the load was approximately 43 kN, three vertical cracks appeared in the two loading points and at the span, and the cracks extended upward to a height of approximately 5 cm. When the load reached 50 kN, cracks began to appear on both sides of the loading point and were basically symmetrically distributed. When the load reached approximately 95 kN, the steel bar began to yield. The crack development of the beam began to accelerate, and the stiffness of the beam decreased. As the load continued to increase, small cracks began to propagate at the bottom of the midspan and penetrate slowly with the adjacent cracks. A scattered inclined crack gradually appeared on the flexural-shear region near the loading point. When the load was 140 kN, the width of the crack near the left loading point reached 0.99 mm. When the load increased to approximately 176 kN, the concrete in the compression zone began to peel and slowly bulged. As the load increased, the bulge became increasingly large, and finally, the concrete in the compression zone was crushed (approximately 194 kN), and the test was stopped.

(2) L-2

When the load was 40 kN, three cracks were found in the bottom of beam L-2 corresponding to the two loading points and the midspan, and the crack spacing was approximately 28 cm. At 55 kN, a second batch of cracks appeared on the midspan and at the two loading points, and the crack width of the latter was relatively small. The cracks propagated toward the top and widened evenly as the load increased. When the load reached approximately 87 kN, the steel bar began to yield, and then the midspan deflection and crack development became faster. When the load was 160 kN, the maximum crack width at the two loading points was 1.03 mm and 1.05 mm. The concrete in the compression zone began to bulge when the load reached 180 kN. At this point, the adjacent cracks on the bottom surface had penetrated to each other, and horizontal cracks were formed. When the load reached 203 kN, the concrete in the compression zone was crushed, and the load dropped sharply. The failure mode of the beam is shown in Fig. 7.

(3) L-3

The number of cracks in L-3 is smaller than that in L-1 and L-2, which was caused by the three longitudinal bars of beam L-3 being

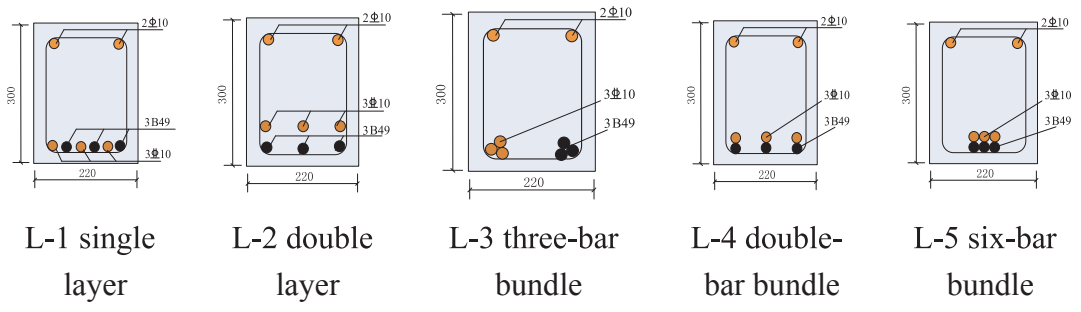

Fig. 3. Different reinforcement methods for the concrete beams (unit: mm).

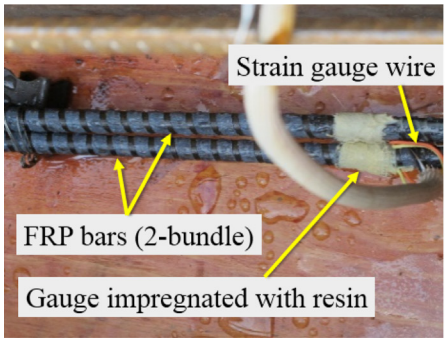

(a) Attached strain gauge

(b) Casting and maintenance of the concrete

Fig. 4. Attaching the strain gauges and casting the test beams.

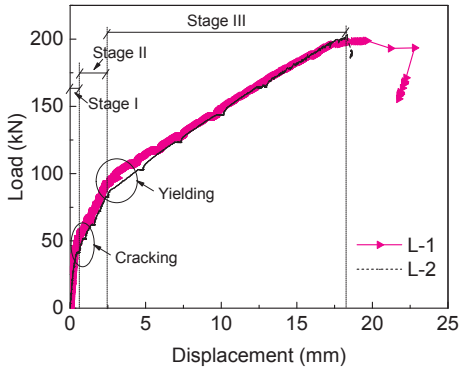

Fig. 5. Load-deflection curves of L-1 and L-2.

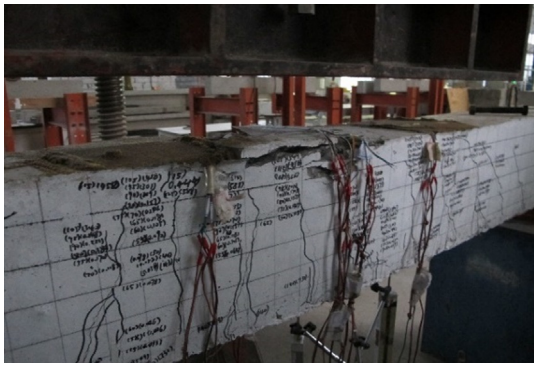

Fig. 6. Failure mode of beam L-1.

concentrated into one bundle. When the load reached approximately 47 kN, the first crack was found in the midspan, and the height of this crack reached approximately 9 cm. Then, the second and third cracks began to appear near the bottom of the beam at the two loading points. When the load reached approximately 100 kN, the tensile steel bar began to yield, and small cracks appeared near the main crack. At this point, the deflection increased rapidly. The crack at the bottom of the beam was widened and gradually penetrated with the adjacent cracks, and the bottom surface formed a transverse crack. When the load was140 kN, the width of the crack near the left loading point was approximately 1.45 mm. When the load was approximately 179 kN, the concrete in the compression zone cracked and gradually formed a bulge. When the load was approximately 205 kN, the concrete in the compression zone crushed (Fig. 8).

(4) L-4

When the load reached approximately 40 kN, beam L-4 had three vertical cracks near the bottom of the corresponding beam at the midspan and the two loading points. At approximately 50 kN, cracks began to appear in the beam shear-flexural section. When the load reached approximately 91 kN, the midspan displacement increased rapidly, and the crack widened rapidly and gradually propagated to the top of the beam. When the load was 140 kN, the width of the crack near the right loading point was 1.62 mm. The cracks no longer propagated upwards when the load reached approximately 190 kN, and the concrete in the compression zone had transverse cracks and began to peel off. When the load reached 214 kN, the concrete in the compression zone crushed (Fig. 9).

(5) L-5

The number of cracks in beam L-5 was less than that in the other four beams. The cracking load was 38 kN, and three cracks were observed simultaneously in the pure bending section, which were located at the midspan (1 crack) and two loading points (one crack each). When the load reached 98 kN, the strain of the longitudinal bar and the midspan displacement suddenly increased, but the load increased slowly. The overall distribution of the cracks was relatively uniform, but the crack width development was uneven, and the cracks near the right loading point developed faster than the other cracks. When the

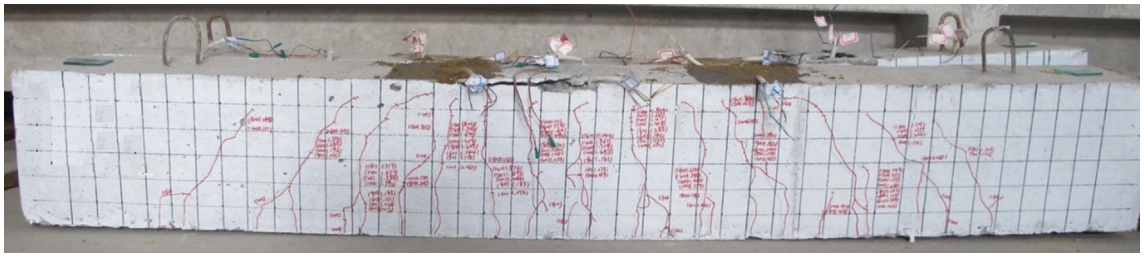

Fig. 7. Failure mode of beam L-2.

Fig. 8. Failure mode of beam L-3.

load was increased to approximately 214 kN, the concrete in the compression zone crushed (Fig. 10).

3.2. Crack development

The widths of the main cracks of the five beams developed as the load increased, as shown in Fig. 11.

The crack widths of beams L-1 through L-4 increased linearly as the load increased in the early stage (before 80 kN). After the concrete beam yielded, the rate of increase in the crack width was relatively faster. The bottom of the main crack began to bifurcate and slowly penetrated with the adjacent cracks, forming a horizontal crack on the concrete cover. The slow development of cracks in beams L-1 and L-2 was mainly due to the large bonding area between the longitudinal reinforcement and the concrete when the distributed reinforcement was used. Moreover, the distributed arrangement of the longitudinal reinforcement can achieve a relatively high bond strength. The cracks of beams L-3, L-4 and L-5 developed faster than those of beams L-1 and L-2, especially L-5, which had a larger crack width under the same load; the number of cracks in beams L-3 and L-5 were 14 and 8, respectively. These findings are mainly due to the change in the longitudinal bars from the dispersed arrangement to the concentrated bundle, which resulted in a smaller bonding area between the longitudinal bars and the surrounding concrete, and an earlier bond-slip occurred.

3.3. Load-displacement curve

The load-displacement curves of the concrete beams are illustrated in Fig. 5 (L-1 and L-2) and Fig. 12 (L-3, L-4, and L-5). Obvious secondary stiffness after yielding can be found, and the secondary stiffness was affected by the reinforcement form. Fig. 5 shows that the curves have two turning points: one is the cracking point, and the other is the yield point. After the beam cracked, the slope of the curve (the stiffness of the beam) decreased. After the steel bar yielded, the stiffness of the beam was further reduced, and the midspan deflection increased rapidly. The loads of the cracking points of beams L-1 and L-2 were similar to each other, which were 43 kN and 40 kN, respectively; the cracking deflections of L-1 and L-2 were 0.335 mm and 0.437 mm, respectively. Moreover, the yield point and the ultimate point of the two beams were relatively close. Compared with the single-layer reinforcement beam (L-1), the double-layer distributed reinforcement (L-2) method slightly reduced the lever arm of the steel bar in the tension zone, but the overall performance of the beam was hardly reduced.

The load-deflection curves of beams L-3, L-4, and L-5 are shown in Fig. 12. Similar to the curves of ordinary nonbundled beams (L-1 and L-2), the load-deflection curves of these beams have two turning points due to concrete cracking and steel yielding. Before the beam cracked, the three curves basically coincided with each other; after cracking and yielding, the stiffness of beam L-4 was relatively larger than that of beams L-3 and L-5, which showed the significant influence of the bonding performance on the load-displacement behavior.

The characteristic values of the cracking point, yield point, peak load point and ultimate point of each beam are shown in Table 2. The load deflection curves of L-1 and L-2 are basically the same, and the corresponding characteristic values are similar to each other. The cracking displacements of beams L-1 and L-2 are relatively close, which are both approximately 0.3 mm. The cracking displacements of beams L-3 and L-5 are similar (approximately 0.64 mm), which are significantly larger than the cracking deflection of beam L-4. It is worth noting that due to the stress redistribution, the deflection of beam L-5 increases sharply from 0.63 mm to 1.67 mm after cracking. The cracking load of L-5 increases slightly from 38 kN to 41.56 kN. This behavior is mainly due to the smaller bonding area between the longitudinal reinforcement of beam L-5 and the surrounding concrete, which causes a large relative slip after cracking.

The yield displacements of beams L-3 and L-5 are 6 mm and 4.8 mm, respectively, which are greater than that of beam L-4 (2.6 mm); these yield displacements are mainly determined by the reinforcement bundle type. The displacements of L-3 and L-5 at the ultimate load are 36.4 mm and 43.9 mm, respectively, which are both greater than that of L-4 (20.3 mm). The reason for this phenomenon is similar to the difference in the yielding point.

The peak loads of beams L-3, L-4, and L-5 are 205 kN, 214 kN and 215 kN, respectively, which are greater than the ultimate loads of beams L-1 and L-2, which are 196 kN and 203 kN, respectively. These results show that the ultimate bearing capacity of the bundled composite reinforced concrete beam is not smaller than that of the ordinary distributed reinforcement beam, and the ultimate moment (load) was enhanced due to the increased ultimate curvature of the section.

3.4. Strain distribution

The strain developments of the FRP bar and steel bar of beam L-1 are shown in Fig. 13. Due to concrete cracking and steel yielding, a

Fig. 9. Failure mode of beam L-4.

Fig. 10. Failure mode of beam L-5.

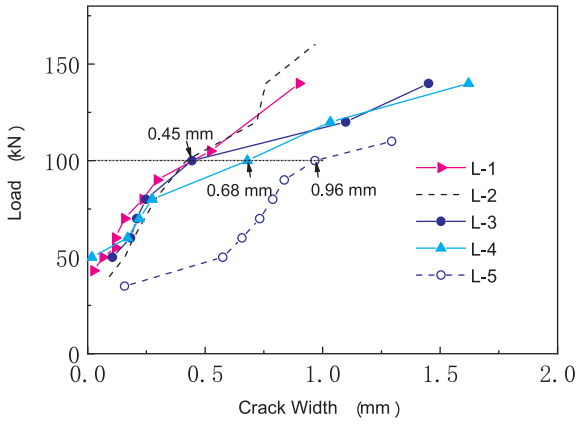

Fig. 11. Comparison of the maximum crack width of each beam.

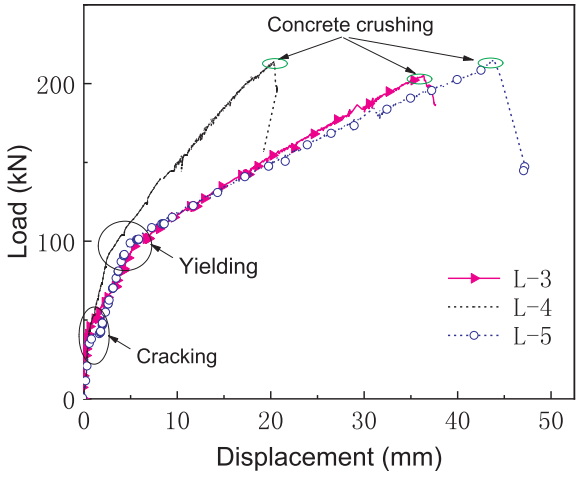

Fig. 12. Load-deflection curves of L-3, L-4 and L-5.

Table 2
Test results of the concrete beams.

Beam number	Cracking point		Yielding point		Peak point		Ultimate point	
	P_{cr} (kN)	δ_{cr} (mm)	P_y (kN)	δ_y (mm)	P_p (kN)	δ_p (mm)	P_u (kN)	δ_u (mm)
L-1	45	0.29	93	2.5	196	17.0	194	22.8
L-2	35	0.31	92	2.8	203	18.4	203	18.4
L-3	47	0.66	103	6.0	205	36.4	205	36.4
L-4	42.5	0.50	99	2.6	214	20.3	214	20.3
L-5	38	0.63	101	4.8	215	43.9	215	43.9

rapid strain increase occurred. The strain in the pure bending region is shown in Fig. 13(a), and the FRP strain F1 and the steel strain C1 are approximately completely coincident before 1000 $\mu\varepsilon$. From the strain development along the length of the beam in Fig. 13(b), it can be seen that under the same load, due to the increase in the section moment, the strain of the FRP bar increases as the distance from the support increases. Especially after the steel bar yielded, the FRP strain of the corresponding section increased rapidly as the load increased.

Since the strain gauges were partially damaged during the specimen casting process, only the data from beam L-1 and beam L-4 are compared in this paper. The strain of the FRP bar in beam L-4 is shown in Fig. 14. The results show that the strains of F2 and F3 in the pure bending section are approximately completely coincident (the strain development trend of steel A1/A3 is similar), and the strain increase in the pure bending section due to cracking is slightly larger than the corresponding FRP strain (Fig. 14a). At 92 kN, the rate of increase in the FRP strain (F1, F2) in the pure bending section rapidly increased due to the steel bar yielding, and the strain gauge of the FRP bar at the F4 position indicated the yield of the corresponding section of the steel bar when the load reached 112 kN (Fig. 14(b)). When the load reached the ultimate load, the corresponding strain of the FRP bar was much smaller than the rupture strain (23500 $\mu\varepsilon$), which indicates that the FRP bar remained elastic.

3.5. Secondary stiffness and ductility

Based on the test results shown in Table 2, the characteristic points of the concrete beam can be obtained (Fig. 15), such as the postcracking stiffness (before yielding) $K_{\text{aftercrack}}$, the initial equivalent stiffness K_{initial}, and the secondary stiffness $K_{\text{afteryield}}$, which can be calculated with the following equations.

$$K_{\text{afterCrack}} = \frac{P_y - P_{cr}}{\delta_y - \delta_{cr}} \tag{2}$$

$$K_{\text{afterYield}} = \frac{P_p - P_y}{\delta_p - \delta_y} \tag{3}$$

$$K_{\text{initial}} = \frac{P_y}{\delta_y} \tag{4}$$

Then, the secondary stiffness ratio of the concrete beam can be obtained:

$$r_b = K_{\text{afteryield}}/K_{\text{initial}} \tag{5}$$

The calculated indicators of the beams are shown in Table 3. The stiffness of the beam decreases with increasing longitudinal reinforcement concentration. The stiffness weakening due to cracking is obvious. The postcracking stiffness ($K_{\text{aftercrack}}$) of L-3 and L-5 was 48% and 69% of that of L-1, respectively. When the steel bar yielded, the secondary stiffness of L-3 and L-5 had a similar development trend, and the value of L-3 and L-5 was less than 50% of that of L-1. Because L-5 had a smaller bonding area than L-3, the secondary stiffness of L-5 was slightly smaller than that of L-3. The initial stiffness of the beam can be obtained by connecting the yield point and the coordinate origin. The initial stiffness of the double-layered beam L-2 was 86% of that of the single-layered beam L-1, whereas the initial stiffness of L-4 was not much different from that of the single-layered beam L-1 (101%).

The secondary stiffness ratio (r_b) of L-2 was 17% higher than that of L-1. The secondary stiffness ratios of beams L-3, L-4, and L-5 were 104%, 91%, and 73% of that of L-1, respectively. These results

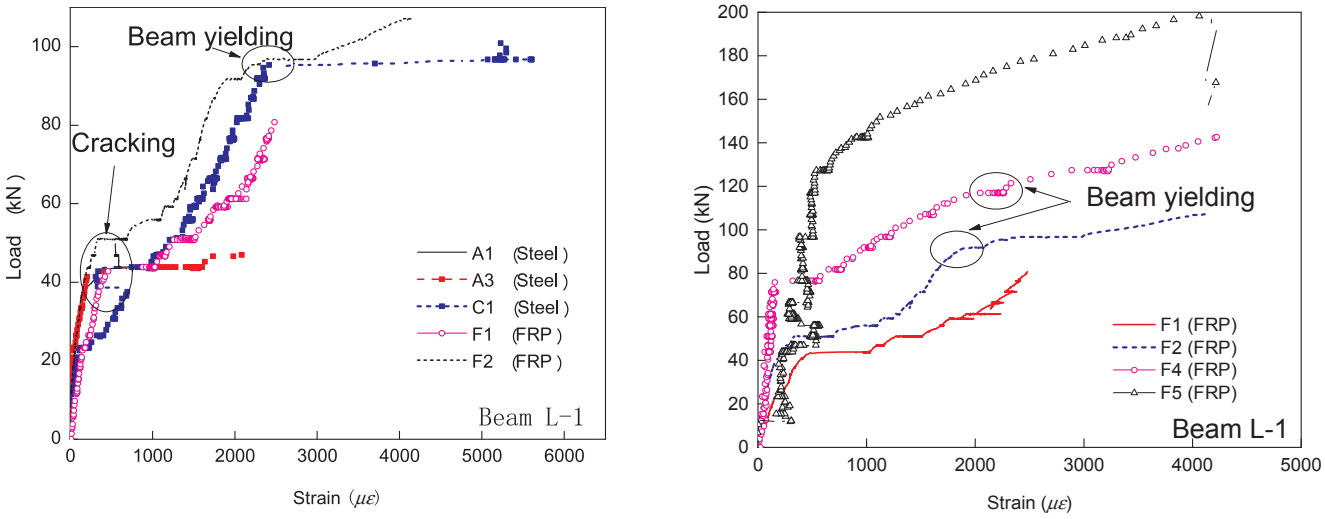

(a) Strain of the pure bending region

(b) Strain of the FRP bar

Fig. 13. Strain of beam L-1.

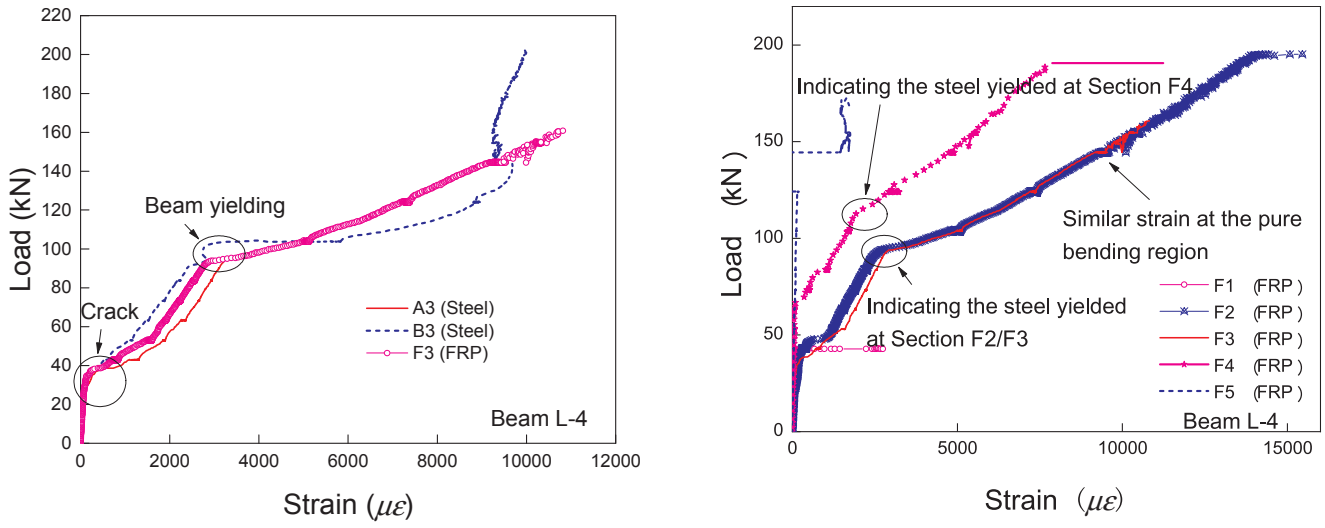

(a) Strain of the FRP bar and steel bar in the pure bending region

(b) FRP strain of beam L-4

Fig. 14. Strain of beam L-4.

preliminarily indicate that the number of concentrated reinforcements less than or equal to the three can ensure that the secondary stiffness ratio is no less than 90% of that of the single-layer reinforcement beam (L-1).

The ductility of the structure refers to the deformation capacity from the start of yielding to the maximum bearing capacity or when the load did not significantly decrease after yielding (80% or 85% of the peak load). The greater the ductility is, the greater the ultimate deformation capacity, and the structure will be relatively safer under the same load. The displacement ductility (μ_δ) can be obtained according to the ultimate displacement and the yield displacement ratio, and the energy ductility (μ_E) can be obtained according to the area of the load-displacement skeleton curve envelope (Fig. 15).

$$\mu_\delta = \frac{\delta_u}{\delta_y} \tag{6}$$

$$\mu_E = \frac{A_u}{A_y} \tag{7}$$

where A_y and A_u are the envelope area of the coordinate origin to the yield point and the envelope area of the coordinate origin to the ultimate point, respectively.

In contrast to a normal RC beam, the energy ductility can take into account the effect of the secondary stiffness caused by the high strength of the FRP, whereas the secondary stiffness of a normal RC beam is close to zero. The displacement ductility and energy ductility of beams with different reinforcement methods are shown in Table 3. In this paper, all the displacement ductility μ_δ values of the composite reinforced beams are greater than 6. The displacement ductility of L-5 is 9.14, and the displacement ductility of L-3 is the smallest (6.05); however, this value is still greater than the displacement ductility of the FRP-reinforced RC beam presented by Oudah [31] (less than 6). After the load reaches the maximum value, beam L-1 has a platform, which may be caused by the local slip of the FRP bar in the ultimate stage, so that the area of the load displacement envelope of L-1 is the largest, and the corresponding energy ductility reaches 28. When the other four beams reach the maximum load, the test machine automatically stops

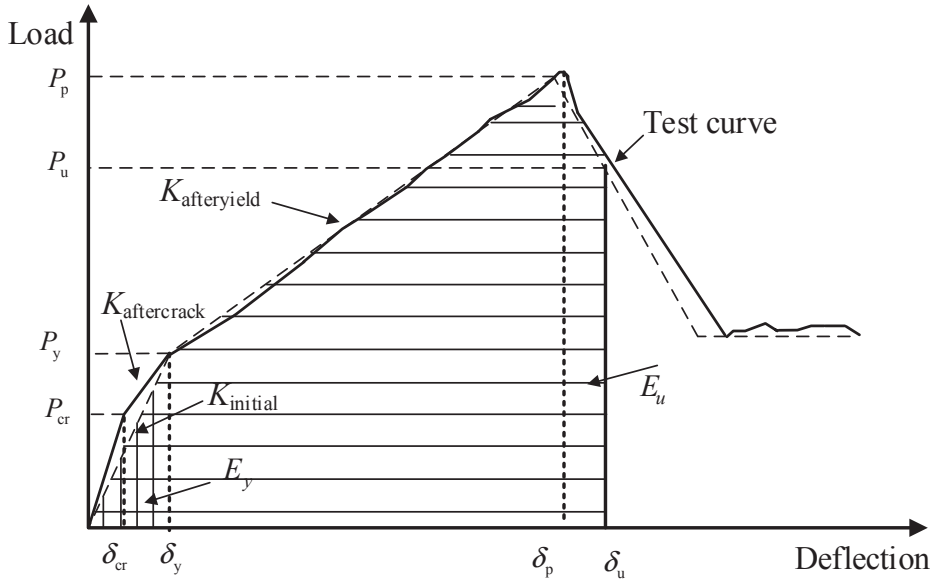

Fig. 15. Schematic diagram of different ductility indexes.

Table 3
Stiffness and ductility coefficient of each beam.

Beam number	$K_{aftercrack}$	$K_{afteryield}$	$K_{initial}$	r_b	μ_δ	$^{*}r_1$	μ_E	$^{**}r_2$
L-1	21.92	7.09	37.50	0.19	9.19	1.00	28.00	1.00
L-2	22.44	7.16	32.28	0.22	6.44	0.70	17.46	0.62
L-3	10.47	3.36	17.14	0.20	6.05	0.66	15.11	0.54
L-4	26.75	6.51	37.92	0.17	7.82	0.85	21.63	0.77
L-5	15.11	2.92	21.04	0.14	9.14	0.99	25.48	0.91

* $r_1 = \mu_\delta/\mu_{\delta\_L\text{-}1}$.
** $r_2 = \mu_E/\mu_{E\_L\text{-}1}$.

due to concrete crushing, and the corresponding maximum load is also taken as the ultimate point. The energy ductility of beam L-3 is the smallest (15.11), which is 54% of that of L-1. The energy ductility of beam L-5, in which six longitudinal bars are concentrated together, reaches 25.48, which is 91% of that of beam L-1. The load-displacement curve (Fig. 12) also shows that the ultimate displacement of L-5 is relatively large.

4. Conclusion

Based on the four-point bending test of two common hybrid reinforced concrete beams and three bundled hybrid reinforced concrete beams, the crack development, load-displacement curve, strain development and ductility index are analyzed. The following conclusions are obtained:

(1) As the number of bundled bars in the concrete beam increases, the number of cracks decreases and the corresponding crack width increases significantly. The concrete beams with bundled longitudinal reinforcement had approximately symmetrically distributed cracks, and the crack width developed faster after the yielding of the steel bars.
(2) After the steel bar in the concrete beam yields, the load can still steadily increase, and a significant and stable secondary stiffness appears. Due to the degradation of the bond behavior, the secondary stiffnesses of beams L-3 and L-5 are smaller than those of the distributed reinforcement beams L-1 and L-2. Concrete cracking and steel yielding can cause a rapid strain increase in the longitudinal bars. Due to the existence of the FRP bar, the plastic development of the steel bar is partially suppressed, and the length of the tensile steel bar that reaches the tensile yield strength becomes longer.
(3) At the yield point and the ultimate point of the concrete beam, the displacement of the beam with bundled reinforcement is much larger than that of the beam with distributed reinforcement, and the ultimate displacement of the former could be even twice that of the latter; however, the ultimate load capacities of the former and the latter were similar. The reason for this discrepancy in ultimate displacement is that the bonding area between the longitudinal reinforcement and the concrete is smaller in the bundled reinforcement beam than in the distributed reinforcement beam, and the bond strength of the former is also lower. All of the displacement ductilities of the concrete beams in this paper are greater than 6, and the energy ductilities are greater than 15.

Declaration of Competing Interest

There is no competing interest.

Acknowledgements

The authors acknowledge the financial support from the National Natural Science Foundation of China (Nos. 51778130, 51708106, 51525801) and project funding from the Priority Academic Program Development of Jiangsu Higher Education Institutions (CE01-2-3). The authors also appreciate the discussion with Jiakai Zhou at Nanjing Forestry University (China) and Dr. Yang and Zhiwei Miao at Southeast University (China).

Appendix A. Supplementary material

Supplementary data to this article can be found online at https://doi.org/10.1016/j.engstruct.2019.109443.

References

[1] Priestley MJN. Overview of PRESSS research program. PCI 1991;36(4):50–7.
[2] Yee AA. Structural and economic benefits of precast/prestressed concrete construction. PCI J 2001;46(4):34–42.
[3] Lu C, Dong B, Pan J, Shan Q, Hanif A, Yin W. An investigation on the behavior of a new connection for precast structures under reverse cyclic loading. Eng Struct 2018;169:131–40.
[4] Jiang C, Wu Y, Dai M. Degradation of steel-to-concrete bond due to corrosion. Constr Build Mater 2018;158:1073–80.
[5] Qu W, Zhang X, Huang H. Flexural behavior of concrete beams reinforced with

hybrid (GFRP and steel) bars. J Compos Constr 2009;13(5):350–9.
[6] Saikia B, Thomas J, Ramaswamy A, Rao K. Performance of hybrid rebars as longitudinal reinforcement in normal strength concrete. Mater Struct 2005;38(10):857–64.
[7] Leung HY, Balendran RV. Flexural behaviour of concrete beams internally reinforced with GFRP rods and steel rebars. Struct Surv 2003;21(4):146–57.
[8] Lau D, Pam HJ. Experimental study of hybrid FRP reinforced concrete beams. Eng Struct 2010;32:3857–65.
[9] Safan MA. Flexural behavior and design of steel-GFRP reinforced concrete beams. ACI Mater J 2013;110(6):677–85.
[10] ACI 440.1R-06, Guide for the design and construction of concrete reinforced with FRP bars. American Concrete Institute (ACI), Detroit, Michigan, USA, 2006.
[11] Jiang C, Wu YF, Wu G. Plastic hinge length of FRP confined square RC columns. J Compos Constr 2014;18(4):4014003–12.
[12] Feng D, Xie S, Deng W, Ding Z. Probabilistic failure analysis of reinforced concrete beam-column sub-assemblage under column removal scenario. Eng Fail Anal 2019;100:381–92.
[13] Kawashima K. Seismic performance of RC bridge piers in Japan: an evaluation after the 1995 Hyogo-ken nanbu earthquake. Prog Struct Eng Mater 2000;2(1):82–91.
[14] Ruiz-Garcia J, Miranda E. Residual displacement ratios for assessment of existing structures. Earthq Eng Struct D 2006;35(3):315–36.
[15] Feng DC, Wang Z, Wu G. Progressive collapse performance analysis of precast reinforced concrete structures. Struct Des Tall Special Buildings 2019;28(5):e1588.
[16] Pettinga D, Christopoulos C, Pampanin S, Priestley N. Effectiveness of simple approaches in mitigating residual deformations in buildings. Earthq Eng Struct D 2007;36(12):1763–83.
[17] Nanni A, Henneke MJ, Okamoto T. Behaviour of concrete beams with hybrid reinforcement. Constr Build Mater 1994;8(2):89–95.
[18] Wu ZS, Iwashita K, Hayashi K, Higuchi T, Murakami S, Koseki Y. Strengthening prestressed-concrete girders with externally prestressed PBO fiber reinforced polymer sheets. J Reinf Plast Comp 2003;22(14):1269–86.
[19] Wu G, Wu ZS, Luo YB, Sun ZY, Hu XQ. Mechanical properties of steel-FRP composite bar under uniaxial and cyclic tensile loads. J Mater Civil Eng 2010;22(10):1056–66.
[20] Wu G, Sun ZY, Wu ZS, Luo YB. Mechanical properties of steel-FRP composite bars (SFCBs) and performance of SFCB reinforced concrete structures. Adv Struct Eng 2012;15(4):625–35.
[21] Wei Y, Zhang X, Wu G, Zhou Y. Behaviour of concrete confined by both steel spirals and fiber-reinforced polymer under axial load. Compos Struct 2018;192:577–91.
[22] Sun ZY, Yang Y, Qin WH, Ren ST, Wu G. Experimental study on flexural behavior of concrete beams reinforced by steel-fiber reinforced polymer composite bars. J Reinf Plast Comp 2012;31(24):53–61.
[23] Sun Z, Wu G, Zhang J, Zeng YH, Xiao W. Experimental study on concrete columns reinforced by hybrid steel-fiber reinforced polymer (FRP) bars under horizontal cyclic loading. Constr Build Mater 2017;130:202–11.
[24] Pang L, Qu W, Zhu P, Xu J. Design propositions for hybrid FRP-steel reinforced concrete beams. J Compos Constr 2015;10-1061:4015086.
[25] Kara IF, Ashour AF, Köroğlu MA. Flexural behavior of hybrid FRP/steel reinforced concrete beams. Compos Struct 2015;129:111–21.
[26] Dundar C, Tanrikulu AK, Frosch RJ. Prediction of load–deflection behavior of multi-span FRP and steel reinforced concrete beams. Compos Struct 2015;132:680–93.
[27] Unsal I, Tokgoz S, Tokgoz S, Cagatay IH, Dundar C. A study on load-deflection behavior of two-span continuous concrete beams reinforced with GFRP and steel bars. Struct Eng Mech 2017;63(5):629–37.
[28] Han SW, Lee CS, Shin M, Lee K. Cyclic performance of precast coupling beams with bundled diagonal reinforcement. Eng Struct 2015;93:142–51.
[29] ACI 318-11. Building code requirements for structural concrete (ACI 318-11), American Concrete Institude, Farmington Hills, MicHigan, USA; 2011.
[30] BS EN 12390-3. Testing hardened concrete. In: Part 3: Compressive Strength of Test Specimens. BSI, London, UK; 2002.
[31] Oudah F, El-Hacha R. A new ductility model of reinforced concrete beams strengthened using fiber reinforced polymer reinforcement. Compos Part B: Eng 2012;43(8):3338–47.